Ultrathin Plasmonic Tungsten Oxide Quantum Wells with Controllable Free Carrier Densities

Gyanaranjan Prusty,[1,#] Jacob T. Lee,[1,#] Soenke Seifert,[2] Barry B. Muhoberac,[1] and Rajesh Sardar*[,1,3]

[1]Department of Chemistry and Chemical Biology, Indiana University-Purdue University Indianapolis, 402 N. Blackford Street, Indianapolis, Indiana 46202, United States

[2]X-ray Science Division, Argonne National Laboratory, Argonne, Illinois 60439, United States

[3]Integrated Nanosystems Development Institute, Indiana University-Purdue University Indianapolis, 423 W. Michigan Street, Indianapolis, Indiana 46202, United States

Supporting Information Placeholder

ABSTRACT: We report the colloidal synthesis of ~3 tungsten-oxygen (W-O) layer thick (~1 nm), two-dimensional (2D) WO_{3-x} nanoplatelets (NPLs) (x ~ 0.55 – 1.03), which display tunable near-infrared localized surface plasmon resonances (LSPR) spectra and high free electron density (N_e) that arises predominantly from their large shape factor. Importantly, the W to O composition ratios inferred from their LSPR measurements show much higher percentage of oxygen vacancies than those determined by X-ray diffraction analysis, suggesting that the aspect ratio of ultrathin WO_{3-x} NPLs is the key to producing an unprecedentedly large N_e, although synthesis temperature is also an independent factor. We find that NPL formation is kinetically controlled, whereas thermodynamic parameter manipulation leads to N_e as high as 4.13 X 10^{22} cm^{-3}, which is close to that of plasmonic noble metals, and thus our oxide-based nanostructures can be considered as *quasi-metallic*. The unique structural properties of 2D nanomaterials along with the high N_e of WO_{3-x} NPLs provide an attractive alternative to plasmonic noble metal nanostructures for energy conversions photochromic nanodevices.

Impressively, the discovery of atomically-thin graphene[1, 2] has completely transformed much material science research involving two-dimensional (2D) nanostructures. By deconvoluting fundamental structure-composition-property relationships, novel electronic and charge transport properties have been created with 2D transition metal dichalcogenides, metal chalcogenides, MXenes, and perovskite nanostructures for advanced solid-state device fabrication.[3, 4] By altering chemical compositions and physical characteristics of nanostructures, new optoelectronic properties emerge that are not achievable in bulk. Among many exotic properties, localized surface plasmon resonance (LSPR),[5] which originates from the collective oscillation of surface bound charges from incident light, is unique, because these plasmon charges can be utilized in photovoltaic, photocatalytic, and photo-thermal therapy applications, as well as bio- and molecular sensing.[6-13]

LSPR properties of nanostructures are mostly controlled by free carrier densities that depend on their size, shape, and dielectric medium.[7, 14] Discovery of LSPR properties and high free carrier densities (10^{22} -10^{23} cm^{-3}) in metals such resulted in tremendous progress in various aspects of nanoscience research. Doped metal oxides (e.g., In_2O_3, Al_2O_3, CdO, ZnO, etc.)[15-19] display LSPR properties, modulated by controlling dopant concentrations.[20] Desirable dispersion relationships[21, 22] and excellent charge transport abilities of 2D plasmonic nanostructures make them attractive candidates for optoelectronic-based applications. Herein, we report the LSPR properties of colloidally-synthesized, ultrathin (~3-W-O layer thick) tungsten oxide quantum wells[23] in the shape of nanoplatelets (NPLs) that can be tuned over 1200-1800 nm in the near-infrared (NIR). We chose tungsten oxide for synthesis because this composition has unmatched potential to display high-temperature superconductivity, fast ion transport, and extremely large magnetoresistance that will lead to various applications such as smart windows, spintronics, quantum computing, and energy storage.[24]

In this communication, tungsten oxide NPLs were synthesized colloidally from the oxidative decomposition of tungsten (V) ethoxide in the presence of myristic acid (MA) and oleylamine (OLA) at 270 ^{O}C. Transmission electron microscopy (TEM) analysis of the purified product, which produces a dark blue colloidal solution in carbon tetrachloride (CCl_4), shows the formation of platelet-type structures with 21.2 and 7.0 nm length and width, respectively (see **Figure 1A &B**, and **S1)**. The geometry of these NPLs resembles metal chalcogenide NPLs.[25] We measured the thickness of tungsten oxide NPLs by Guinier analysis of small angle X-ray scattering (SAXS) spectrum which yields ~1 nm (**Figure 1C**). We also calculated the thickness of NPLs from the TEM analysis and determined it to be 1.0 ± 0.2 nm, see **Figure S2**. The structural characterization provides an aspect ratio (width-to-thickness) of 7.0. As illustrated in **Figure 1D**, X-ray diffraction (XRD) analysis of NPLs confirms monoclinic lattice structure with

This is the author's manuscript of the article published in final edited form as:
Prusty, G., Lee, J. T., Seifert, S., Muhoberac, B. B., & Sardar, R. (2020). Ultrathin Plasmonic Tungsten Oxide Quantum Wells with Controllable Free Carrier Densities. Journal of the American Chemical Society. https://doi.org/10.1021/jacs.9b13909

predicted composition of $W_{18}O_{49}$, which is a stoichiometric of $WO_{2.72}$.[26]

Due to the broad XRD peak of ultrathin NPLs, it is difficult to absolutely determine the precise stoichiometry of our tungsten oxides NPLs. LSPR-based calculations[27, 28] however, can provide a nearly quantitative stoichiometric ratio of plasmonic nanostructures. We determined that our calculated tungsten oxide NPLs stoichiometry diverse substantially from the XRD-derived value discussed below. Therefore, we refer to our synthesized NPLs as WO_{3-x}. Considering each W-O layer as 0.37 nm thick, our tungsten oxide NPLs contain ~3 layers. **Table S1** lists reaction conditions for the synthesis of WO_{3-x} NPLs. Although, one-dimensional (1D) nanostructures composed of $WO_{2.72}$ have been reported,[29-31] this is first example of the synthesis of 2D NPLs consisting of different lattice stoichiometries. Detailed investigation of the LSPR properties of previously reported 1D nanostructures is also lacking.

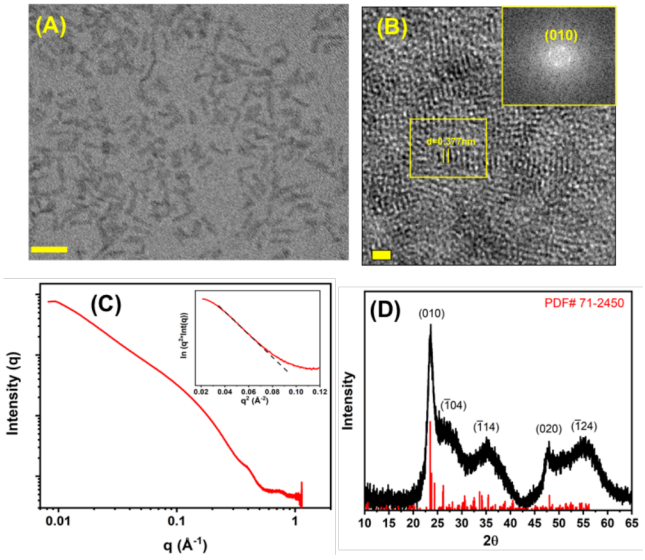

Figure 1. (A) Low and (B) high-resolution TEM images of WO_{3-x} NPLs. The scale bars in (A) and (B) are 10 and 5 nm, respectively. The inset in (B) shows FFT of (010) plane. The yellow box shows *d-spacing* of 0.377 nm. (C) SAXS spectrum and (D) XRD pattern of NPLs. The inset in (C) shows Guinier fit to determine the thickness.

WO_{3-x} NPLs exhibit a remarkably well-defined, characteristic LSPR peak (λ_{LSPR}) at ~1470 nm, **Figure 2A**. To confirm that this NIR response is due to crystal lattice oxygen vacancies that generate free carrier electrons and not from scattering, impurities, or absorption by local defects,[28, 32] we examined the band position as a function of solvent refractive index that red shifts as refractive indices increases (**Figure 2B and S3**). This direction is in agreement with nanostructures that display LSPR properties.[5] Our WO_{3-x} NPLs show LSPR sensitivity of 330 nm/refractive index unit (nm/RIU), which is higher than previously reported for $WO_{2.83}$ nanorods[24] and Cs_xWO_3 nanostructures,32 and is comparable to 2D plasmonic metal nanostructures.[7, 33]

This relatively higher RIU sensitivity of our WO_{3-x} NPLs compared to other tungsten oxide-based nanostructures is from the larger shape factor, κ, of 2D nanostructures versus their 1D counterparts.[34] The polarizability of plasmonic charge carriers at the nanostructure-solvent interface is much greater when κ is higher and a minute medium dielectric change should significantly alter the LSPR properties.[34] Ultrathin edges and sharp corners of WO_{3-x} NPLs are expected to contain a high free carrier density that should produce a large near-field enhancement of surface plasmon,[35] and corresponding large LSPR response, as demonstrated for 2D Au[8, 10, 33] and Ag nanoprisms.[7, 36] Our ^{1}H NMR and FTIR characterizations confirm both MA and OLA surface passivating ligands (**Figure S4 &S5**). Because of oxygen-containing passivating ligands, it is difficult to determine the W to O ratios by other techniques, such as X-ray photoelectron or electron paramagnetic resonance spectroscopy. Perhaps, a Drude treatment of the dielectric function is the only method to precisely determine the stoichiometry of WO_{3-x} NPLs.

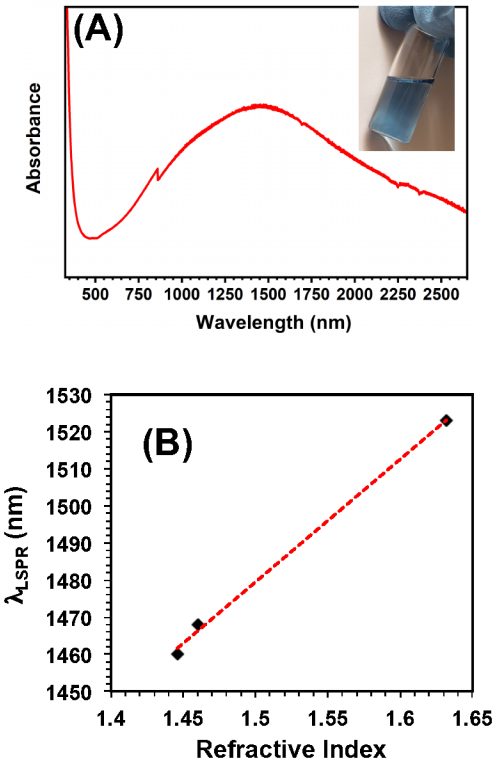

Figure 2. (A) UV-Vis-NIR spectrum of WO_{3-x} NPLs in CCl_4. The inset shows photograph of WO_{3-x} NPLs in $CHCl_3$. (B) The dependence of λ_{LSPR} maximum on the index of refraction of solvent.

Combining our experimentally determined λ_{LSPR} energy WO_{3-x} NPLs with the Drude model for bulk materials, we can calculate free electron density (N_e). Eq. 1 represents the relation used between LSPR frequency (ω_{LSPR}) and bulk plasma oscillation frequency of electrons (ω_p) for tungsten oxide with a high frequency dielectric constant (ϵ_∞) of 4.5.

$$\omega_{LSPR} = \sqrt{\frac{\omega_p^2}{\epsilon_\infty - \varepsilon_r} - \gamma^2} \quad (1)$$

Where ε_r denotes the real part of the complex dielectric function, ε, of the plasmonic nanostructures.

$$\varepsilon_r = -\kappa\varepsilon_m \quad (2)$$

Here ε_m is the dielectric constant of the surrounding medium, taken as the bulk refractive index (CCl_4 = 2.24). The electrons of the nanostructure oscillate from the incident field, and the motion is collisionally damped with a bulk collision frequency γ, 0.736 eV, see **Table S1**. Finally, ω_p depends on N_e as

$$\omega_p^2 = \frac{N_e e^2}{\varepsilon_o m_e} \quad (3)$$

where, m_e is the effective mass of an electron and ε_0 is the permittivity of free space. For WO_{3-x} we used m_e = 1.2 m_0,[26] where m_0 is the rest mass of an electron. With the assumption that WO_{3-x} NPLs are oblate spheroids with an aspect ratio of 7.0 (shape factor of 9.6) and based on the above-mentioned values, we calculate N_e to be 3.36 X 10^{22} cm^{-3}. This value is nearly five-fold higher than the stoichiometrically determined N_e for $WO_{2.83}$ nanorods (N_e = 6.3 X 10^{21} cm^{-3}),[24] and is more than two order of magnitude higher than 2D metal chalcogenide nanodisks (N_e = 1.0 X 10^{20} cm^{-3}).[27, 37] With the assumption that two electrons in the WO_{3-x} crystal lattice originate from a fully ionized oxygen deficiency and by utilizing the LSPR properties of WO_{3-x} NPLs, we determine the oxygen deficiency as 27.7% providing the stoichiometric composition of NPLs as $WO_{2.17}$ (see **Table S2**). Therefore, the calculated stoichiometry of the NPL lattice shows more oxygen deficiency than the predicted from the XRD analysis. This could be the reason underlying the unprecedentedly high free carrier densities of our synthesized WO_{3-x} NPLs. We should also mention that the calculated oxygen deficiency, and hence the NPL lattice stoichiometry could be slightly overestimated because of the intrinsic and inhomogeneous line-broadening that arises from shape dispersion, as previously reported for LSPR active metal chalcogenide nanocrystals.[28]

Nanostructure LSPR properties of strongly depend on their size and shape,[7, 20] so we investigated the ability of temperature to manipulate thermodynamic growth regime and prepare anisotropically-shaped WO_{3-x} nanostructures.[38, 39] To our surprise, WO_{3-x} NPLs of a few atomic layers thickness are also formed when the reaction was carried out at 230 and 300 ^{O}C (**Figure 3A-B**) with both displaying monoclinic crystal structure (**Figure S6 & S7**).

Importantly, the λ_{LSPR} blue shifts with increasing reaction temperature (**Figure 3C**). The N_e values of WO_{3-x} NPLs synthesized at 300 and 230 ^{O}C are calculated to be 3.95 X 10^{22} and 2.53 X 10^{22} cm^{-3}, respectively (see **Figure 3D**), which correspond to $WO_{2.02}$ and $WO_{2.37}$ stoichiometries. The larger N_e from 300 ^{O}C synthesis closely approximates plasmonic metals, so our nanostructures can be considered as *"quasi-metallic"*.[40] The unprecedentedly large N_e of WO_{3-x} NPLs is better explained by their ultrathin shape where a large percentage of oxygen atoms reside on the surface and sharp corners and edges. These atoms should be highly susceptible to fast ionization at high temperature, creating more oxygen vacancies and thus dramatically increasing N_e. It is well known for plasmonic noble metal nanostructures that λ_{LSPR} red shifts as their aspect ratio increases.[33, 34, 36] Based on our calculations, WO_{3-x} NPLs synthesized at 300 ^{O}C should display the most red-shifted λ_{LSPR} because of their highest aspect ratio. However, we observe opposite LSPR effects (see **Table S1**). In contrast, Eq. 2 and 3 suggest that with an increase in N_e, the λ_{LSPR} should blue shift, which we observe here. Thus, both the shape factor and collision frequency must be carefully included to generalize the LSPR-related metal oxide nanostructure properties. Nevertheless, to the best of our knowledge, this is the highest N_e value reported for LSPR-active metal oxide nanostructures including recently reported spherical ReO_3 NCs.[41] Finally, we estimated the direct optical band gap of WO_{3-x} NPLs from a plot of $(\alpha h\nu)^2$ versus $h\nu$ (Tauc plot). We detecte a monotonic increase in the band gap energy with increasing reaction temperature (**Figure S8**) attributable to the Burstein-Moss shift.[42] The band gap energy is also in agreement with increasing N_e values for NPLs synthesized at different temperatures.

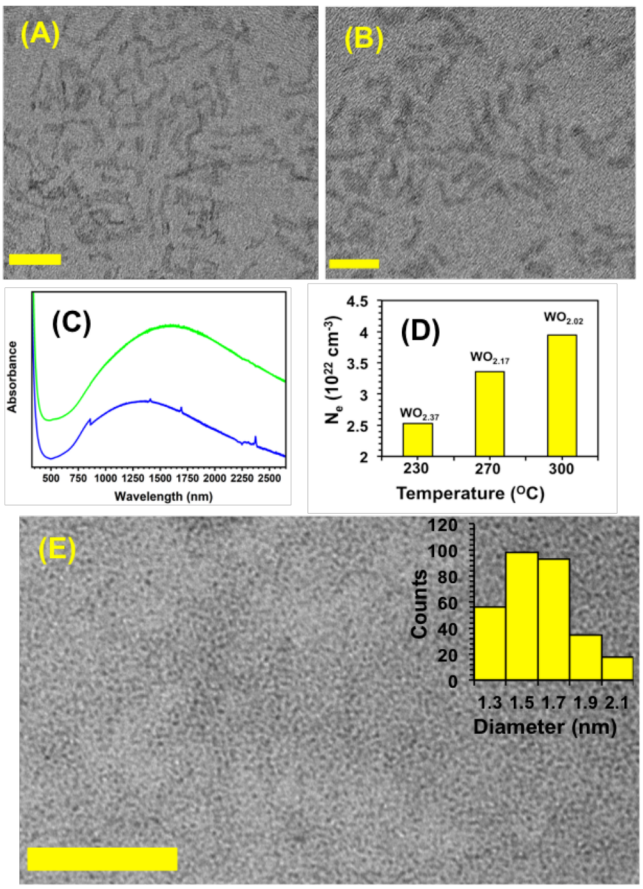

Figure 3. HRTEM images of $WO_{2.72}$ NPLs in CCl_4 synthesized at (A) 230 and (B) 300 ^{O}C. Scale bars are 20 nm. (C) UV-Vis-NIR spectrum of WO_{3-x} NPLs in CCl_4 synthesized at (green) 230 and (blue) 300 ^{O}C. (D) The plot of free carrier densities of WO_{3-x} NPLs versus reaction temperature. (E) A representative TEM image of spherical WO_{3-x} NCs. The scale bar is 50 nm. The inset shows a histogram of the size distribution.

We also investigated the effects of surface passivating ligands controlling the kinetic growth regime at a particular temperature[38, 39, 43] on the shape/size of the nanostructure formed, and thus the N_e of tungsten oxide nanostructures. We determine that at 270 ^{O}C: (1) The presence of both long hydrocarbon chain amines and acids together in the reaction mixture is required for WO_{3-x} NPL synthesis. (2) Formation of tungsten oxide nanostructures is not observed when the reaction is carried out in the presence of OLA alone. (3) Nearly monodispersed, spherical, WO_{3-x} NCs are formed (**Figure 3E and S9**)

when the synthesis is conducted in the presence of just MA. Supporting information **Table S1-S2** contains reaction conditions, morphology, dimensions and representative N_e values of tungsten oxide nanostructures. Based on the experimentally determined λ_{LSPR} of ~985 nm for average 1.6 nm diameter WO_{3-x} NCs, we calculate a N_e value of 2.68 X 10^{22} cm^{-3}. Our synthesis hypothesis is that initially formed spherical NCs are passivated with aliphatic carboxylate ligands and a bilayer structure is formed between the aliphatic chains of amine and acid ligands through van der Waals (vdW) interactions.44, 45 Particularly, vdW interactions and chain interdigitation induce mesoscale growth where individual spherical, WO_{3-x} NCs fuse together and transform into NPLs (**Figure 3**).

In conclusion, we have demonstrated the colloidal synthesis of ~1 nm thick WO_{3-x} NPLs with N_e value as high as 4.13 X 10^{22} cm^{-3} (**Table S2**). The reaction temperature plays a significant role in manipulating the oxygen vacancies, which control the overall N_e values. Their LSPR properties can be tuned by manipulating the N_e values without changing crystal stoichiometry. Together, our work has the unique potential to expand research in light harvesting schemes[11-13] and plasmon-assisted photo-thermal therapy.[46]

ASSOCIATED CONTENT

Supporting Information. Materials and methods, experimental details, additional TEM images, histograms, UV-vis-NIR, XRD, SAXS, NMR and FTIR spectra, and tables.

AUTHORS CONTRIBUTION

G.P and J.T.L. contributed equally to this work.

AUTHOR INFORMATION

Corresponding Author

rsardar@iupui.edu

Notes

The authors declare no competing financial interest

ACKNOWLEDGMENT

Financial support was provided by NSF (DMR-1747582). This research used resources of the Advanced Photon Source, a U.S. Department of Energy (DOE) User Facility operated for the DOE Office of Science by Argonne National Laboratory under Contract DEAC02-06CH11357. TEM analyses were conducted at the Electron Microscopy Core Facility, Indiana University School of Medicine.

REFERENCES

1. Geim, A. K.; Novoselov, K. S. The rise of graphene. *Nat. Mater.* **2007**, *6*, 183-191.
2. Novoselov, K. S.; Geim, A. K.; Morozov, S. V.; Jiang, D.; Zhang, Y.; Dubonos, S. V.; Grigorieva, I. V.; Firsov, A. A. Electric Field Effect in Atomically Thin Carbon Films. *Science* **2004**, *306*, 666-669.
3. Nasilowski, M.; Mahler, B.; Lhuillier, E.; Ithurria, S.; Dubertret, B. Two-Dimensional Colloidal Nanocrystals. *Chem. Rev.* **2016**, *116*, 10934-10982.
4. Tan, C.; Cao, X.; Wu, X.-J.; He, Q.; Yang, J.; Zhang, X.; Chen, J.; Zhao, W.; Han, S.; Nam, G.-H., *et al.* Recent Advances in Ultrathin Two-Dimensional Nanomaterials. *Chem. Rev.* **2017**, *117*, 6225-6331.
5. Mulvaney, P. Surface Plasmon Spectroscopy of Nanosized Metal Particles. *Langmuir* **1996**, *12*, 788-800.
6. Joshi, G. K.; Deitz-McElyea, S.; Liyanage, T.; Lawrence, K.; Mali, S.; Sardar, R.; Korc, M. Label-Free Nanoplasmonic-Based Short Noncoding RNA Sensing at Attomolar Concentrations Allows for Quantitative and Highly Specific Assay of MicroRNA-10b in Biological Fluids and Circulating Exosomes. *ACS Nano* **2015**, *9*, 11075-11089.
7. Mayer, K. M.; Hafner, J. H. Localized Surface Plasmon Resonance Sensors. *Chem. Rev.* **2011**, *111*, 3828-3857.
8. Joshi, G. K.; Blodgett, K. N.; Muhoberac, B. B.; Johnson, M. A.; Smith, K. A.; Sardar, R. Ultrasensitive Photoreversible Molecular Sensors of Azobenzene-Functionalized Plasmonic Nanoantennas. *Nano Lett.* **2014**, *14*, 532-540.
9. Joshi, G. K.; Deitz-McElyea, S.; Johnson, M.; Mali, S.; Korc, M.; Sardar, R. Highly Specific Plasmonic Biosensors for Ultrasensitive MicroRNA Detection in Plasma from Pancreatic Cancer Patients. *Nano Lett.* **2014**, *14*, 6955-6963.
10. Liyanage, T.; Nagaraju, M.; Johnson, M.; Muhoberac, B. B.; Sardar, R. Reversible Tuning of the Plasmoelectric Effect in Noble Metal Nanostructures Through Manipulation of Organic Ligand Energy Levels. *Nano Lett.* **2019**, *20*, 192-200.
11. Atwater, H. A.; Polman, A. Plasmonics for improved photovoltaic devices. *Nat. Mater.* **2010**, *9*, 205-213.
12. Linic, S.; Christopher, P.; Ingram, D. B. Plasmonic-metal nanostructures for efficient conversion of solar to chemical energy. *Nat. Mater.* **2011**, *10*, 911-921.
13. Zhou, L.; Swearer, D. F.; Zhang, C.; Robatjazi, H.; Zhao, H.; Henderson, L.; Dong, L.; Christopher, P.; Carter, E. A.; Nordlander, P., *et al.* Quantifying hot carrier and thermal contributions in plasmonic photocatalysis. *Science* **2018**, *362*, 69-72.
14. Halas, N. J.; Lal, S.; Chang, W.-S.; Link, S.; Nordlander, P. Plasmons in Strongly Coupled Metallic Nanostructures. *Chem. Rev.* **2011**, *111*, 3913-3961.
15. Kanehara, M.; Koike, H.; Yoshinaga, T.; Teranishi, T. Indium tin oxide nanoparticles with compositionally tunable surface plasmon resonance frequencies in the near-IR region. *J. Am. Chem. Soc.* **2009**, *131*, 17736-17737.
16. Schimpf, A. M.; Lounis, S. D.; Runnerstrom, E. L.; Milliron, D. J.; Gamelin, D. R. Redox Chemistries and Plasmon Energies of Photodoped In2O3 and Sn-Doped In2O3 (ITO) Nanocrystals. *J. Am. Chem. Soc.* **2015**, *137*, 518-524.
17. Ye, X.; Fei, J.; Diroll, B. T.; Paik, T.; Murray, C. B. Expanding the spectral tunability of plasmonic resonances in doped metal-oxide nanocrystals through cooperative cation-anion codoping. *J. Am. Chem. Soc.* **2014**, *136*, 11680-11686.
18. Faucheaux, J. A.; Jain, P. K. Plasmons in Photocharged ZnO Nanocrystals Revealing the Nature of Charge Dynamics. *J. Phys. Chem. Lett.* **2013**, *4*, 3024-3030.
19. Gordon, T. R.; Paik, T.; Klein, D. R.; Naik, G. V.; Caglayan, H.; Boltasseva, A.; Murray, C. B. Shape-dependent plasmonic response and directed self-assembly in a new semiconductor building block, indium-doped cadmium oxide (ICO). *Nano Lett.* **2013**, *13*, 2857-2863.
20. Agrawal, A.; Cho, S. H.; Zandi, O.; Ghosh, S.; Johns, R. W.; Milliron, D. J. Localized Surface Plasmon Resonance in Semiconductor Nanocrystals. *Chem. Rev.* **2018**, *118*, 3121-3207.
21. Wang, Y.; Ou, J. Z.; Chrimes, A. F.; Carey, B. J.; Daeneke, T.; Alsaif, M. M. Y. A.; Mortazavi, M.; Zhuiykov, S.; Medhekar, N.; Bhaskaran, M., *et al.* Plasmon Resonances of Highly Doped Two-Dimensional MoS2. *Nano. Lett.* **2015**, *15*, 883-890.
22. Scholz, A.; Stauber, T.; Schliemann, J. Plasmons and screening in a monolayer of MoS${}_{2}$. *Phys. Rev. B* **2013**, *88*, 035135.
23. Pelton, M.; Ithurria, S.; Schaller, R. D.; Dolzhnikov, D. S.; Talapin, D. V. Carrier Cooling in Colloidal Quantum Wells. *Nano Lett.* **2012**, *12*, 6158-6163.
24. Manthiram, K.; Alivisatos, A. P. Tunable localized surface plasmon resonances in tungsten oxide nanocrystals. *J. Am. Chem. Soc.* **2012**, *134*, 3995-3998.

25. Ithurria, S.; Dubertret, B. Quasi 2D Colloidal CdSe Platelets with Thicknesses Controlled at the Atomic Level. *J. Am. Chem. Soc.* **2008**, *130*, 16504-16505.
26. Molenda, J.; Kubik, A. Electrical Properties of Nonstoichiometric WO3−y at Temperatures 77 to 300 K. *phys. status solidi b* **1995**, *191*, 471-478.
27. Hsu, S. W.; On, K.; Tao, A. R. Localized surface plasmon resonances of anisotropic semiconductor nanocrystals. *J. Am. Chem. Soc.* **2011**, *133*, 19072-19075.
28. Luther, J. M.; Jain, P. K.; Ewers, T.; Alivisatos, A. P. Localized surface plasmon resonances arising from free carriers in doped quantum dots. *Nat. Mater.* **2011**, *10*, 361-366.
29. Liu, J.; Margeat, O.; Dachraoui, W.; Liu, X.; Fahlman, M.; Ackermann, J. Gram-Scale Synthesis of Ultrathin Tungsten Oxide Nanowires and their Aspect Ratio-Dependent Photocatalytic Activity. *Adv. Func. Mater.* **2014**, *24*, 6029-6037.
30. Yella, A.; Tahir, M. N.; Meuer, S.; Zentel, R.; Berger, R.; Panthöfer, M.; Tremel, W. Synthesis, Characterization, and Hierarchical Organization of Tungsten Oxide Nanorods: Spreading Driven by Marangoni Flow. *J. Am. Chem. Soc.* **2009**, *131*, 17566-17575.
31. Heo, S.; Kim, J.; Ong, G. K.; Milliron, D. J. Template-Free Mesoporous Electrochromic Films on Flexible Substrates from Tungsten Oxide Nanorods. *Nano Lett.* **2017**, *17*, 5756-5761.
32. Mattox, T. M.; Bergerud, A.; Agrawal, A.; Milliron, D. J. Influence of Shape on the Surface Plasmon Resonance of Tungsten Bronze Nanocrystals. *Chem. Mater.* **2014**, *26*, 1779-1784.
33. Joshi, G. K.; McClory, P. J.; Muhoberac, B. B.; Kumbhar, A.; Smith, K. A.; Sardar, R. Designing Efficient Localized Surface Plasmon Resonance-Based Sensing Platforms: Optimization of Sensor Response by Controlling the Edge Length of Gold Nanoprisms. *J. Phys. Chem. C* **2012**, *116*, 20990-21000.
34. Jain, P. K.; El-Sayed, M. A. Surface Plasmon Resonance Sensitivity of Metal Nanostructures: Physical Basis and Universal Scaling in Metal Nanoshells. *J. Phys. Chem. C* **2007**, *111*, 17451-17454.
35. Kim, J.; Agrawal, A.; Krieg, F.; Bergerud, A.; Milliron, D. J. The Interplay of Shape and Crystalline Anisotropies in Plasmonic Semiconductor Nanocrystals. *Nano Lett.* **2016**, *16*, 3879-3884.
36. Khan, A. U.; Zhao, S.; Liu, G. Key Parameter Controlling the Sensitivity of Plasmonic Metal Nanoparticles: Aspect Ratio. *J. Phys. Chem. C* **2016**, *120*, 19353-19364.
37. Liu, M.; Xue, X.; Ghosh, C.; Liu, X.; Liu, Y.; Furlani, E. P.; Swihart, M. T.; Prasad, P. N. Room-Temperature Synthesis of Covellite Nanoplatelets with Broadly Tunable Localized Surface Plasmon Resonance. *Chem. Mater.* **2015**, *27*, 2584-2590.
38. Jun, Y.-w.; Choi, J.-s.; Cheon, J. Shape Control of Semiconductor and Metal Oxide Nanocrystals through Nonhydrolytic Colloidal Routes. *Angew. Chem. Int. Ed.* **2006**, *45*, 3414-3439.
39. Xia, Y.; Xia, X.; Peng, H.-C. Shape-Controlled Synthesis of Colloidal Metal Nanocrystals: Thermodynamic versus Kinetic Products. *J. Am. Chem. Soc.* **2015**, *137*, 7947-7966.
40. Hoffman, A. J.; Alekseyev, L.; Howard, S. S.; Franz, K. J.; Wasserman, D.; Podolskiy, V. A.; Narimanov, E. E.; Sivco, D. L.; Gmachl, C. Negative refraction in semiconductor metamaterials. *Nat. Mater.* **2007**, *6*, 946-950.
41. Ghosh, S.; Lu, H.-C.; Cho, S. H.; Maruvada, T.; Price, M. C.; Milliron, D. J. Colloidal ReO3 Nanocrystals: Extra Re d-Electron Instigating a Plasmonic Response. *J. Am. Chem. Soc.* **2019**, *141*, 16331-16343.
42. Burstein, E. Anomalous Optical Absorption Limit in InSb. *Phys. Rev.* **1954**, *93*, 632-633.
43. Yin, Y.; Alivisatos, A. P. Colloidal nanocrystal synthesis and the organic-inorganic interface. *Nature* **2005**, *437*, 664-670.
44. Cölfen, H.; Mann, S. Higher-Order Organization by Mesoscale Self-Assembly and Transformation of Hybrid Nanostructures. *Angew. Chem. Int. Ed.* **2003**, *42*, 2350-2365.
45. Teunis, M. B.; Johnson, M. A.; Muhoberac, B. B.; Seifert, S.; Sardar, R. Programmable Colloidal Approach to Hierarchical Structures of Methylammonium Lead Bromide Perovskite Nanocrystals with Bright Photoluminescent Properties. *Chem. Mater.* **2017**, *29*, 3526-3537.
46. Gibbs, S. L.; Staller, C. M.; Milliron, D. J. Surface Depletion Layers in Plasmonic Metal Oxide Nanocrystals. *Acc. Chem. Res.* **2019**, *52*, 2516-2524.

Insert Table of Contents artwork here